Energy Advances

ROYAL SOCIETY OF CHEMISTRY

PAPER

View Article Online
View Journal

Cite this: DOI: 10.1039/d6ya00033a

Synergistic enhancement of the properties of composite solid electrolytes *via* PAN and *in situ* SiO_2 for all-solid-state lithium batteries

Hun Lee [a] and Sung Yeon Hwang*[b]

Received 12th February 2026,
Accepted 1st May 2026

DOI: 10.1039/d6ya00033a

rsc.li/energy-advances

This work presents the fabrication of a composite solid polymer electrolyte (CSE) by blending poly(ethylene oxide) (PEO) with polyacrylonitrile (PAN) and incorporating SiO_2 nanoparticles generated *via* an *in situ* process. The addition of PAN effectively disrupts the crystalline structure of PEO and increases the amorphous phase and polymer chain flexibility, which facilitates improved lithium ion mobility. The *in situ* formation of SiO_2 *via* tetraethyl orthosilicate (TEOS) hydrolysis ensures the uniform dispersion of ceramic fillers, which enhances the mechanical properties, thermal stability, and ion-transport pathways. The optimized CSE-15 sample demonstrates a notable ionic conductivity of 3.81×10^{-4} S cm^{-1} at an elevated temperature and a lithium-ion transference number of 0.36, indicative of efficient lithium transport. Electrochemical testing reveals a wide electrochemical stability window, extending to 4.5 V (*vs.* Li/Li^+), while the lithium symmetric cells exhibit prolonged cycling stability and the effective suppression of dendritic growth. Furthermore, full cell tests using $LiFePO_4$ as the cathode show a high specific capacity of 151.4 mA h g^{-1}, with a Coulombic efficiency of 99.8% over 150 cycles at 0.5C and 60 °C. The synergistic effect of polymer blending and *in situ* filler incorporation is found to optimize the balance between ionic conductivity, mechanical integrity, and interfacial compatibility, which are critical parameters for advancing solid-state lithium batteries. These findings provide valuable insights into the rational design of composite electrolytes. Therefore, the obtained CSE is a promising candidate for developing safe and high-performance lithium metal batteries.

1. Introduction

Currently, lithium-ion secondary batteries are widely used across a broad range of applications, from portable electronic devices, such as smartphones, laptops, and gaming consoles, to electric vehicles (EVs) and large-scale energy storage systems (ESS), owing to their high energy density, excellent charge/discharge cycle performance, long lifespan, and high output voltage.[1,2] There is a growing demand for devices with high efficiency and energy density, which imposes high technical requirements and needs continuous performance improvements. However, conventional lithium-ion batteries are struggling to meet the rapidly rising performance demands across various fields. In particular, typical lithium-ion batteries use liquid organic electrolytes, which cause several critical challenges, including electrolyte leakage and side reactions with electrodes. Furthermore, these batteries suffer from severe capacity decay, rate capability degradation, and accelerated lithium dendrite formation under low-temperature (LT) operation, necessitating a more systematic understanding of the electrolyte behavior in extreme environments.[3] These issues lead to capacity fading, decomposition under high-voltage operation, and even safety hazards, such as fire or explosion, due to the flammable nature of the liquid electrolytes.[4–9] To address these problems, the use of solid-state electrolytes (SSEs) is considered a promising solution as they significantly enhance battery safety and cycle life by eliminating the inherent risks associated with liquid electrolytes.

Compared with liquid electrolytes, solid-state electrolytes exhibit several advantageous properties, including low flammability, non-volatility, and excellent mechanical and thermal stability.[10–15] Although recent studies have attempted to overcome the limitations of liquid electrolytes through advanced electrolyte engineering by employing novel additives, such as viologens for accelerated lithium-ion migration[16] or LiDFOB/BTFE combinations for enhanced fast-charging,[17] it remains a significant challenge to simultaneously achieve extreme fast-charging, high-voltage stability, and absolute safety. Consequently, solid electrolytes are generally categorized into three main types: inorganic ceramic

[a] Department of Advanced Materials Chemistry, College of Engineering, Cheongju University, 298, Daeseong-ro, Cheongwon-gu, Cheongju-si, Chungcheongbuk-do, 28503, Republic of Korea
[b] Department of Convergent Biotechnology and Advanced Materials Science, Kyung Hee University, Yongin, 17104, Republic of Korea. E-mail: crew75@khu.ac.kr

electrolytes (ICEs),[18–24] polymer-based solid electrolytes (PSEs),[25–30] and composite solid electrolytes (CSEs).[31–38] Among them, ICEs encompass a variety of material types, including garnet-type, NASICON-type, perovskite-type, LISICON-type, and argyrodite-type structures. Due to their superior mechanical properties, high thermal stability, excellent ionic conductivity, and wide electrochemical stability window, ICSs have attracted significant attention. However, their inherent brittleness, along with large interfacial and grain boundary resistance, gives rise to a critical challenge that hinders practical application in all-solid-state battery systems.

In contrast, PSEs offer excellent processability and flexibility, favorable interfacial compatibility, and low flammability. Despite these advantages, their practical applications are limited due to their relatively narrow electrochemical stability window, low ionic conductivity at ambient temperature, and insufficient mechanical strength. Since ionic transport predominantly occurs in the amorphous regions of polymers, the high crystallinity inherent in many polymer matrices significantly impedes ion mobility. To address these limitations, plasticizers are often incorporated into the polymer matrix to form gel polymer electrolytes (GPEs), which enhance ionic conductivity.[39–41] However, the addition of plasticizers generally reduces the mechanical strength, electrochemical stability, and flame resistance of the electrolyte. Many studies have been devoted to enhancing the performance of polymer electrolytes through several approaches, such as polymer blending (*e.g.*, PEO, PAN, PVP, PVDF, and PVDF-HFP), block copolymer formation, polymer chain alignment, and the creation of cross-linked polymer networks.[29,31,42–44] Although many improvements in polymer electrolytes have been achieved through previous research, they still suffer from challenges, including low ionic conductivity at room temperature, oxidative or thermal degradation, and insufficient suppression of lithium dendrite growth.

CSEs have garnered significant research interest in a direction that integrates the advantages of both inorganic ceramic and polymer-based electrolytes. Accordingly, numerous strategies have been developed to fabricate CSEs that can maintain mechanical robustness and interfacial stability with lithium metal without relying on plasticizers. Typically, active ceramic fillers, such as LATP ($Li_{1.3}Al_{0.3}Ti_{1.7}(PO_4)_3$), LLZO ($Li_7La_3Zr_2O_{12}$), and LLTO ($Li_3xLa_2/3–xTiO_3$), are employed as additives.[45–48] These active fillers not only enhance the physical and mechanical properties of the polymer matrix but also actively participate in lithium-ion transport, thereby significantly improving the electrochemical performance of the electrolyte.

One promising strategy for designing CSEs involves incorporating inorganic fillers, such as ZnO, TiO_2, Al_2O_3, and SiO_2, into polymer matrices.[37,49–51] These ceramic fillers possess high specific surface areas and Lewis acid characteristics, which contribute to enhanced lithium-ion conductivity. Specifically, the fillers interrupt the reorganization of polymer chains and reduce crystallinity, thereby facilitating segmental motion and promoting ion transport. Additionally, strong Lewis acid–base interactions between the ionic species in the electrolyte and the functional groups on the filler surface enhance the dissociation of lithium salts and improve the stability of the anions. These effects not only improve the mechanical properties and interfacial contact of the solid electrolyte but also help to suppress the growth of lithium dendrites. Croce and Scrosati[49] demonstrated that the addition of nanosized TiO_2 (13 nm) and Al_2O_3 (5.8 nm) particles to a PEO-$LiClO_4$ matrix increased ionic conductivity from 10^{-8} S cm^{-1} to approximately 1.7×10^{-5} S cm^{-1} at room temperature. This improvement was attributed to the high surface area of the nanoparticles, which effectively suppressed the recrystallization of the polymer upon cooling from the amorphous state. Simultaneously, the mechanical properties of the polymer matrix were also enhanced. In another study,[34] the incorporation of 10 wt% SiO_2 particles (5–10 nm in size) into a PEO-$LiClO_4$ matrix resulted in an initial conductivity of $\sim 10^{-5}$ S cm^{-1} at room temperature. However, this value decreased to $\sim 10^{-6}$ S cm^{-1} after one week, indicating that the suppression of recrystallization was incomplete. Lyu *et al.*[43] achieved a conductivity of 0.8×10^{-4} S cm^{-1} at room temperature by adding succinonitrile (SN) and SiO_2 nanospheres into a PEO matrix. The enhancement was attributed to reduced crystallinity and improved chain mobility induced by the additives. Despite these advances, most conventional fabrication methods for CSEs involve the direct mixing of pre-synthesized ceramic nanoparticles with the polymer matrix. This approach often leads to non-uniform dispersion, particle aggregation, and weak interactions between the fillers and polymer chains, limiting overall performance due to the presence of crystalline regions. To address these interfacial issues, recent studies have explored modified fillers. For instance, incorporating oxygen-vacancy LLZTO (OV-LLZTO) into PEO has been shown to strengthen the bonding with polymer chains, effectively reducing interfacial resistance and preventing PEO crystallization.[52] To overcome the challenges, an *in situ* synthesis approach has been proposed. Lin *et al.*[35] developed a CSE by incorporating monodispersed ultrafine SiO_2 particles into PEO through the *in situ* hydrolysis of TEOS. This method resulted in an ionic conductivity of 4.4×10^{-5} S cm^{-1} at 30 °C. Recent advancements in *in situ* polymerization have further demonstrated the potential to create phase-separated systems that simultaneously enhance interfacial wettability and generate stable, LiF-rich interphases at both electrodes, thereby achieving state-of-the-art electrochemical performance.[53] The *in situ* synthesized SiO_2 particles offer better particle dispersion and more efficient Lewis acid–base interactions compared to simple mechanical mixing, thereby enhancing both the structural and electrochemical properties of the solid polymer electrolyte. As discussed thus far, the incorporation of individual fillers or additives into CSEs improves specific properties, such as ionic conductivity and interfacial contact. However, the overall electrochemical performance of the electrolyte still requires significant enhancement. To maximize these improvements, the adoption of systematic approaches, such as the Design of Experiments (DoE), is essential, as it allows for the exploration of multiple variables and their synergistic interactions, replacing repeated testing strategies.[54] Given that each type of filler and additive functions through different mechanisms and contributes to the performance improvements of solid electrolytes, introducing multiple functional materials simultaneously into the solid electrolyte is

considered an effective strategy. This approach has the potential to achieve synergistic effects that address multiple limitations simultaneously.

In this study, a composite solid polymer electrolyte is developed by appropriately integrating multiple materials to synergistically utilize their properties. Poly(ethylene oxide) (PEO) is selected as the polymer matrix due to its thermoplastic nature, excellent film-forming ability, and good flexibility and adhesiveness, which allow tight interfacial contact with the electrodes. Moreover, the ether oxygen atoms in the PEO polymer chains form coordination complexes with Li^+ ions, providing effective ion transport pathways. PEO also shows good compatibility with lithium salts, such as LiTFSI and $LiClO_4$, leading to the formation of stable composites.[34,55,56] However, the high crystallinity of PEO limits Li^+ mobility, resulting in low ionic conductivity. To address this, polyacrylonitrile (PAN) is introduced *via* blend mixing instead of using succinonitrile (SN), a commonly used plasticizer. While SN has a low molecular weight that weakens the mechanical strength of the polymer matrix, PAN has a high molecular weight that not only suppresses the crystallinity of PEO but also enhances mechanical strength, contributing to the inhibition of lithium dendrite growth.[25,38] Furthermore, PAN exhibits high oxidative, thermal, and electrochemical stability, making it a desirable polymeric additive. The terminal cyano groups ($C\equiv N$) in PAN coordinate with Li^+ ions, promoting ionic migration. However, PAN by itself lacks intrinsic Li^+ conductivity and has limited interaction with lithium salts. Excessive PAN content leads to phase separation within the electrolyte, facilitating non-uniform morphology and reduced ionic conductivity. Therefore, the PAN content is carefully optimized in this study to balance ionic conductivity and mechanical integrity. This balancing act is crucial, as evidenced by recent findings that while high salt concentrations enhance ionic conductivity, low salt concentrations can offer significantly high mechanical stiffness and long cycling life.[57] To further enhance the ionic conductivity and overall electrochemical performance, nanoscale inorganic fillers are incorporated into the electrolyte. SiO_2 nanoparticles expand the amorphous regions in the polymer matrix and form numerous interfacial conduction pathways, which accelerate Li^+ transport. Additionally, SiO_2, as a ceramic filler, contributes to mechanical reinforcement, dimensional stability, thermal resistance, improved electrode–electrolyte interfacial contact, and the suppression of lithium salt decomposition caused by moisture absorption. However, the inert and active ceramic nanoparticle fillers introduced as preformed ceramics often lead to the agglomeration and heterogeneous dispersion of fillers and weak interactions between polymer chains and ceramic particles, thereby limiting further improvements in the conductivity of polymer electrolytes.[35] To ensure the homogeneous dispersion and interfacial chemical stability of the inorganic particles, *in situ* SiO_2 was formed *via* the hydrolysis of TEOS in a PEO/PAN polymer blend solution. Based on this material design strategy, we develop a PEO/PAN-based solid electrolyte containing monodispersed ultrafine SiO_2 particles. The strong chemical and mechanical interactions between the formed SiO_2 spheres and polymer chains successfully suppress the crystallinity of PEO/PAN. Furthermore, the precisely controlled growth of SiO_2 ensures improved particle distribution and monodispersity, increasing the effective surface area for efficient Lewis acid–base interactions. The resulting CSE is characterized using SEM, XRD, and FT-IR analyses. Electrochemical performance is evaluated through AC impedance spectroscopy to determine ionic conductivity; linear sweep voltammetry (LSV) to evaluate electrochemical stability and lithium dendrite suppression; and galvanostatic charge–discharge cycling to investigate specific capacity, Coulombic efficiency, and cycle stability. The fabricated CSE exhibits an ionic conductivity of 3.81×10^{-4} S cm^{-1} at 60 °C, measured in a symmetric stainless steel/electrolyte/stainless steel cell. In a Li/electrolyte/Li symmetric cell, stable cycling is maintained for approximately 150 h at 60 °C and 0.1 mA cm^{-2}, demonstrating excellent interfacial and structural stability. Furthermore, an all-solid-state battery assembled with this electrolyte achieves a high specific capacity of 153.3 mA h g^{-1} at 0.5C and retains 99.8% of its capacity after 150 cycles at 0.5C and 60 °C. These results clearly indicate that the designed composite solid electrolyte is a promising candidate for use in next-generation solid-state lithium-ion batteries.

2. Experimental

2.1. Materials

The materials used in this study are PEO (M_W = 1 000 000, Sigma-Aldrich), PAN (M_W = 150 000, Sigma-Aldrich), lithium bis(trifluoromethanesulfonyl)imide (LiTFSI, 99.95%, MTI-Korea), *N*,*N*-dimethylformamide (DMF, 99.8%, Sigma-Aldrich), tetraethyl orthosilicate (TEOS, 98%, Sigma-Aldrich), hydrochloric acid (HCl, 37%, Sigma-Aldrich), $LiFePO_4$ powder (LFP, 99.9%, MTIKorea), polyvinylidene fluoride (PVDF, HSV900, Arkema Co.), *N*-methylpyrrolidone (NMP, 99.99%, Sigma-Aldrich), carbon black (Ketjenblack EC-600JD, Sigma-Aldrich), and lithium metal foil (MTIKorea). All chemicals were used as received, without further purification.

2.2. Preparation of composite solid electrolyte

The CSE was prepared using a conventional solution casting method. First, LiTFSI and TEOS were sequentially dissolved in DMF under magnetic stirring at room temperature. LiTFSI, being the key component responsible for providing lithium ion conductivity, was first introduced into the solvent to ensure stable dissolution. After LiTFSI was completely dissolved, other components were added to this solution. TEOS formed SiO_2 nanoparticles through hydrolysis and condensation reactions. Once TEOS was added dropwise and stabilized in the solution, HCl was added at a TEOS:HCl molar ratio of 1 : 2 to promote hydrolysis reaction and facilitate the formation of a uniform SiO_2 distribution within the solution. PAN was added to the solution, and the mixture was vigorously stirred at 60 °C for 30 min until fully dissolved. In this process, TEOS was hydrolyzed and condensed to form extremely small SiO_2 nanoparticles. Although SiO_2 is generally insoluble, these nanoparticles were

uniformly dispersed within the PAN solution, allowing it to remain transparent. Next, PEO was added while continuing vigorous stirring, and the solution was stirred at 60 °C for 24 h to obtain a homogeneous solution with a concentration of 6%, where the molar ratio of Li^+ to EO was 1 : 17. For comparison experiments, the mass ratios of PAN to PEO were 0 : 1, 1 : 2, 1 : 5, and 1 : 10. The amount of TEOS added to the solution was adjusted to ensure that it constituted 8% of the total polymer content after conversion to SiO_2. The fully dissolved solution was then scraped onto the polytetrafluoroethylene (PTFE) film sheet. The sample was placed in a dry chamber at 60 °C for 12 h to remove the solvent and was then dried at room temperature for 48 h in order to ensure the complete removal of the residual solvent. Finally, the samples were obtained and stored in a vacuum oven until further use.

2.3. Preparation of a cathode and an all-solid-state battery

The LFP cathode sheets were prepared using a slurry casting method, which involved mixing an active material, binder, conductive additive, and solvent. First, $LiFePO_4$ (80 wt%), PVDF (10 wt%), and carbon black (10 wt%) were added to NMP and stirred into a uniform slurry at room temperature. The prepared slurry was cast onto an aluminum foil using a doctor blade and dried in a vacuum oven at 100 °C for 12 h. The completely dried cathode electrode was cut into circular disks with diameters of 10 mm, and the active material loading was approximately 1.8 mg cm^{-2}. This loading was chosen as it is commonly used in laboratory-scale studies to ensure uniform coating, reproducibility, and reliable electrochemical measurements. For electrochemical analysis, 2032-type coin cells were assembled using the prepared composite solid electrolyte, LFP electrode, lithium metal, and stainless steel in an argon-filled glove box. During the assembly of all cells, spacers were inserted to increase the stacking pressure inside the cell, ensuring that the electrodes and electrolyte were sufficiently in contact.

2.4. Characterization of composite solid electrolyte

In this study, the shape and composition, mechanical properties, crystallinity, and thermal behavior of the material were analyzed using the following equipment. The morphology and elemental composition of CSE were studied by field emission scanning electron microscopy (FE-SEM, MERLIN, Carl Zeiss) equipped with an energy dispersive spectroscopy (EDS) system. The EDS mapping was performed on the surface of the CSE sample. XRD analysis was performed using an X-ray diffractometer (D8 Advance, Bruker) instrument with a scan speed of 4° min^{-1} and a 2θ range from 10° to 60° to determine the crystal structure of CSE. Differential scanning calorimetry (DSC, Q-1000, TA) was used to measure the crystallinity and thermal properties of the electrolyte material in N_2 atmosphere. Fourier transform infrared spectroscopy (FT-IR, Nicolet Summit X, Thermo Fisher) was carried out over a wavelength range of 400–4000 cm^{-1} to analyze the chemical bonding of the components in fabricated CSE. The morphological features and crystalline structures were consistently reproduced across multiple batches, confirming that the *in situ* synthesis of SiO_2 and its integration into the PEO/PAN matrix were highly stable and reliable processes.

2.5. Electrochemical measurements

Electrochemical impedance spectroscopy (EIS) tests were conducted using an impedance spectrometer instrument (ZIVE SP1, WonATech). A symmetric cell, consisting of stainless steel (SS) and CSE (SS/CSE/SS), was assembled to measure the ionic conductivity (σ) in the frequency range from 100 kHz to 0.1 Hz, with a voltage amplitude of 10 mV. Ionic conductivity was calculated using eqn (1) as follows:

$$\sigma = L/(R_b \times S) \quad (1)$$

where L (cm) is the thickness of CSE, R_b is the bulk resistance of the electrolyte, and S represents the contact area between CSE and SS.

The lithium ion transference number (t_{Li^+}) was determined using the chronoamperometry method with a Li/CSE/Li symmetric cell. EIS was conducted before and after DC polarization in the frequency range from 100 kHz to 0.1 Hz at room temperature, with a test voltage of 10 mV applied until the current stabilized. t_{Li^+} was calculated using the Vincent-Evans eqn (2) as follows:

$$t_{Li^+} = I_{ss}(\Delta V - I_0R_0)/I_0(\Delta V - I_{ss}R_{ss}) \quad (2)$$

where I_0 and I_{ss} are the initial and steady-state currents, respectively, ΔV represents the applied voltage, and R_0 and R_{ss} are the impedances before and after polarization, respectively. For electrochemical evaluations, including EIS and lithium-ion transference number measurements, the results were obtained by averaging the data from multiple cells to minimize experimental error and ensure statistical significance.

Linear scanning voltammetry (LSV) was performed using an SS/CSE/Li asymmetric cell to determine the electrochemical stability window of the electrolyte. The potential range was from 2.0 to 5.5 V (*vs.* Li/Li^+) with a scan rate of 1 mV s^{-1} at room temperature. The stripping/plating behavior of CSE was measured using a Li/CSE/Li symmetric cell at a current density of 0.1 mA cm^{-2}. The galvanostatic electrochemical measurements and cycling performances of the asymmetry half-cells (Li/CSE/LFP) were evaluated, with voltage ranges found to be between 2.5 and 4.2 V, using an automatic charge–discharge electrochemical workstation (WBCS 3000L, WonATech). The specific capacities and energy densities were determined by calculating the mass of active materials in the cathode electrode, which were responsible for charge storage and energy release. The electrochemical tests were conducted using independent cells for each condition, and the representative data set is reported.

3. Results and discussion

Fig. 1 schematically illustrates the fabrication process of the composite solid electrolytes. In this study, PEO was selected as the primary polymer matrix due to its ability to facilitate

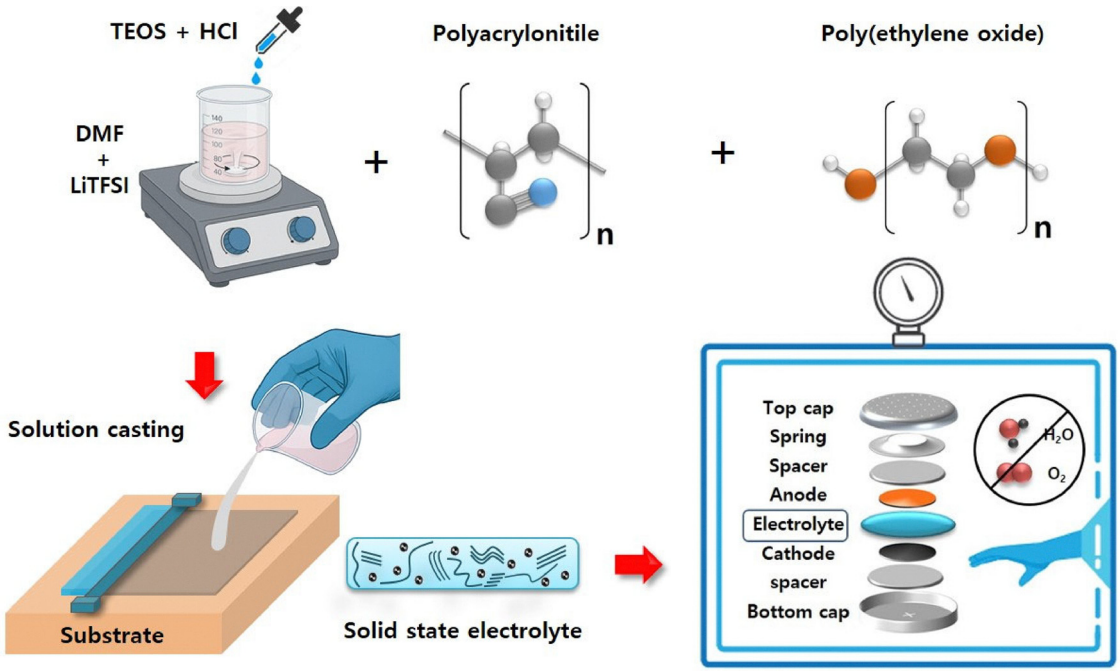

Fig. 1 Schematic of the preparation procedure and cell configuration.

lithium-ion transport and form a continuous ion-conductive phase. The PEO-based solid electrolyte exhibits inherent tackiness, enabling intimate contact with the electrodes during cell assembly, which is further supported by the use of spacers, as illustrated in Fig. 1. It is well known that ionic conductivity in solid polymer electrolytes mainly occurs in the amorphous regions of the polymer matrix.[58] However, the high crystallinity of PEO hinders its ionic conductivity when used alone, which limits its performance as a solid electrolyte. To overcome this limitation and improve the mechanical strength and suppress the crystallinity of PEO, PAN was incorporated through polymer blending. The degree of crystallinity in the blended polymer matrix varies depending on the blending ratio of PAN to PEO.[26,58,59] However, it induces phase separation and disrupts continuous ion-conduction pathways because excessive PAN content leads to a poor interaction with lithium salts.

This can negatively affect both the ionic conductivity and electrochemical stability of the electrolyte. Accordingly, composite solid electrolytes were prepared with PAN : PEO ratios of 0 : 1, 1 : 2, 1 : 5, and 1 : 10 to determine the optimal PAN-to-PEO ratio and analyze the relationship between crystallinity, ionic conductivity, and mechanical properties. The corresponding samples were denoted as CSE-01, CSE-12, CSE-15, and CSE-110, respectively. To further enhance lithium-ion conductivity, LiTFSI was added at a molar ratio. LiTFSI forms coordination complexes with the ether oxygen atoms in the PEO chains, advancing lithium-ion transport and increasing the amorphous content of the polymer, thereby improving the ionic conductivity. However, excessive salt concentration causes the formation of ion pairs or aggregates, which adversely affect ionic mobility. In this study, the EO : Li^+ molar ratio was fixed at 17 : 1, which was widely regarded as optimal for balancing ionic conductivity and crystallinity suppression in solid polymer electrolyte systems. This specific ratio has been shown in previous studies to enhance conductivity while maintaining electrochemical stability across various polymer electrolyte platforms. For example, Fan and Fedkiw[51] reported the conductivity of solution electrolytes containing lithium salts at various molar ratios. Their study showed that composite electrolytes had a high ionic conductivity at room temperature ($\sim 1.5 \times 10^{-5}$ S cm^{-1}), a wide potential window (~ 5.5 V), and relatively stable performance with the Li^+ : EO ratio range from 15 : 1 to 20 : 1. Kim *et al.*[60] prepared a composite electrolyte consisting of PEO, LiTFSI, SN, LLZANO, and LiDFP. They used 16 : 1 as the molar ratio of EO : Li^+ and achieved high ionic conductivities and stable electrochemical performance. Yang *et al.*[32] added LiTFSI to the membrane at an EO : Li^+ ratio of 20 : 1. The resulting electrolyte membrane offered good ionic conductivity and stability against lithium dendrite formation.

In the prepared composite solid electrolytes, SiO_2 inorganic nanoparticles were incorporated *via* a non-aqueous sol–gel process. Previous studies have demonstrated that the optimal SiO_2 content typically ranges from 5% to 10% relative to the total polymer weight.[34,43,51] Within this range, the inorganic fillers effectively promote ion transport by inhibiting polymer recrystallization while maintaining the structural integrity of the membrane. Accordingly, the SiO_2 content in this study was selected as 8% to achieve balanced electrochemical and mechanical properties. This was achieved by the *in situ* hydrolysis of tetraethyl orthosilicate (TEOS) within the polymer matrix using HCl as a catalyst, thereby promoting the uniform distribution of SiO_2 throughout the electrolyte. The *in situ* sol–gel process allowed for strong interfacial interactions between the formed SiO_2 nanospheres and the polymer chains, which

was particularly effective in suppressing the crystallinity of PEO. During the fabrication process, all components were fully dissolved and homogeneously mixed in a single DMF solvent at 60 °C. This processing condition facilitated the uniform nanoscale dispersion of both the polymer matrix and the inorganic SiO_2 particles during electrolyte formation. The consistency of this fabrication protocol was verified through the production of multiple batches, which yielded composite electrolytes with highly uniform and reproducible physical properties. The incorporation of inorganic nanoparticles into polymer electrolytes is generally known to offer several advantages, including enhanced mechanical strength, increased amorphous regions, and extended lithium-ion transport pathways. However, the conventional addition of ceramic fillers often suffers from drawbacks, such as particle aggregation, uneven dispersion, and interfacial incompatibility, which bring about decreased ionic conductivity and poor electrochemical performance. For direct comparison, a control sample (denoted as CSE-p) was also prepared by the mechanical mixing of pre-synthesized SiO_2 nanoparticles with the polymer matrix. In contrast, the *in situ*-generated SiO_2 in this study effectively alleviated these limitations by ensuring homogeneous nanoparticle distribution, improving interfacial compatibility between the polymer and inorganic component, and enhancing both the ionic conductivity and cycling stability of the electrolyte. This approach demonstrated the potential of *in situ* ceramic synthesis as an effective strategy for optimizing the structure and performance of composite solid electrolytes in all-solid-state lithium batteries.

The surface morphology of CSE prepared in this study was examined *via* scanning electron microscopy (SEM). As shown in Fig. 2a–c, the CSE-01, CSE-15, and CSE-110 samples exhibit smooth and uniform surfaces, characterized by compact and dense microstructures without pores. A similar surface morphology was observed for CSE-p (Fig. 2e), which was prepared using pre-synthesized SiO_2, showing no significant differences in surface appearance compared to the *in situ* samples. This suggests that while the surface appearance remains uniform regardless of the SiO_2 incorporation method, the internal dispersion and interfacial interactions may differ significantly, as further investigated through EDS. SEM surface images revealed no visible SiO_2 nanoparticles, suggesting that the particles were well embedded and dispersed within the polymer matrix. The consistent surface uniformity across these samples indicated the excellent film-forming capability of the PEO/PAN polymer blend matrix, which effectively incorporated the inorganic fillers. On the other hand, the CSE-12 sample (Fig. 2d), which contained the highest PAN content, displayed a rough and heterogeneous surface with numerous visible micropores. This result was attributed to excessive PAN incorporation, which likely disrupted uniform mixing within the polymer matrix and hindered proper film formation. Such phase separation and surface roughening have been previously reported as common outcomes of compositional imbalance and weak miscibility between blended polymers.[56,59,61] The electrolyte has to exhibit good flexibility and self-standing characteristics. However, the CSE-12 film demonstrated stiffer and rougher surface features compared to the other samples. This was considered to result from the high PAN content, reducing the overall flexibility of the polymer matrix and interfering with smooth film formation. By comparison, the PAN-free sample (CSE-01) showed excessive stickiness, leading to poor dimensional stability and handling difficulties during cell assembly. The cross-sectional SEM images of the CSE films (Fig. 2f) clearly showed a uniform and symmetric internal morphology, confirming the successful formation of dense and coherent composite electrolytes. Since solid electrolytes must serve both as ion-conducting media and physical separators between electrodes, controlling the thickness of the film is crucial. While a thin film enhances ionic conductivity, it reduces mechanical integrity and is insufficient to suppress the lithium dendrite growth. On the contrary, thick films increase ionic resistance and negatively affect overall cell performance. Therefore, the thickness was optimized to balance mechanical stability and ionic conductivity. The final film thickness was controlled by adjusting the solution volume and casting height during the solution casting process, producing films approximately 80 μm thick.

To analyze the elemental distribution, EDS mapping was conducted on the surface of the CSE sample, as shown in Fig. 2g–j. Fig. 2g shows the non-uniform distribution of Si from a sample prepared by the conventional mechanical mixing of the pre-synthesized SiO_2 nanoparticles. This was attributed to the agglomeration and inhomogeneous dispersion of inorganic particles, leading to unstable electrochemical performance, weak interactions between the fillers and polymer, and limited ionic conductivity. In contrast, the samples where SiO_2 was introduced *via* the *in situ* sol–gel method exhibited a significantly improved and uniform Si distribution. The mapping results of CSE-15 presented here represent the typical elemental distribution observed across various samples, confirming the reproducibility of the homogeneous dispersion. The elemental mapping of Si obtained from EDS analysis (Fig. 2h) confirmed that the inorganic ceramic filler (SiO_2) was homogeneously distributed throughout the polymer matrix. This uniform distribution of the filler was beneficial as it provided continuous pathways for lithium-ion transport, thereby promoting uniform lithium metal deposition. However, the localized agglomeration of inorganic fillers was observed in certain areas. This phenomenon was attributed to local inconsistencies during the hydrolysis and condensation steps of the sol–gel reaction, as well as to variations in solvent evaporation rates. In addition, the inherent aggregation tendency of inorganic nanoparticles played a role in this result. Such issues could potentially be mitigated by the precise control of processing parameters, including pH adjustment, reaction time optimization, and the incorporation of suitable dispersants. Fig. 2i and j demonstrate that sulfur (S) and fluorine (F) elements are uniformly dispersed throughout the polymer matrix, indicating that the LiTFSI salt is evenly distributed in all composite electrolyte samples. This uniform salt distribution ensured consistent lithium-ion transport within the solid electrolyte, minimizing local concentration gradients and preventing electrochemical imbalances. It resulted in improved electrolyte stability, reduced interfacial

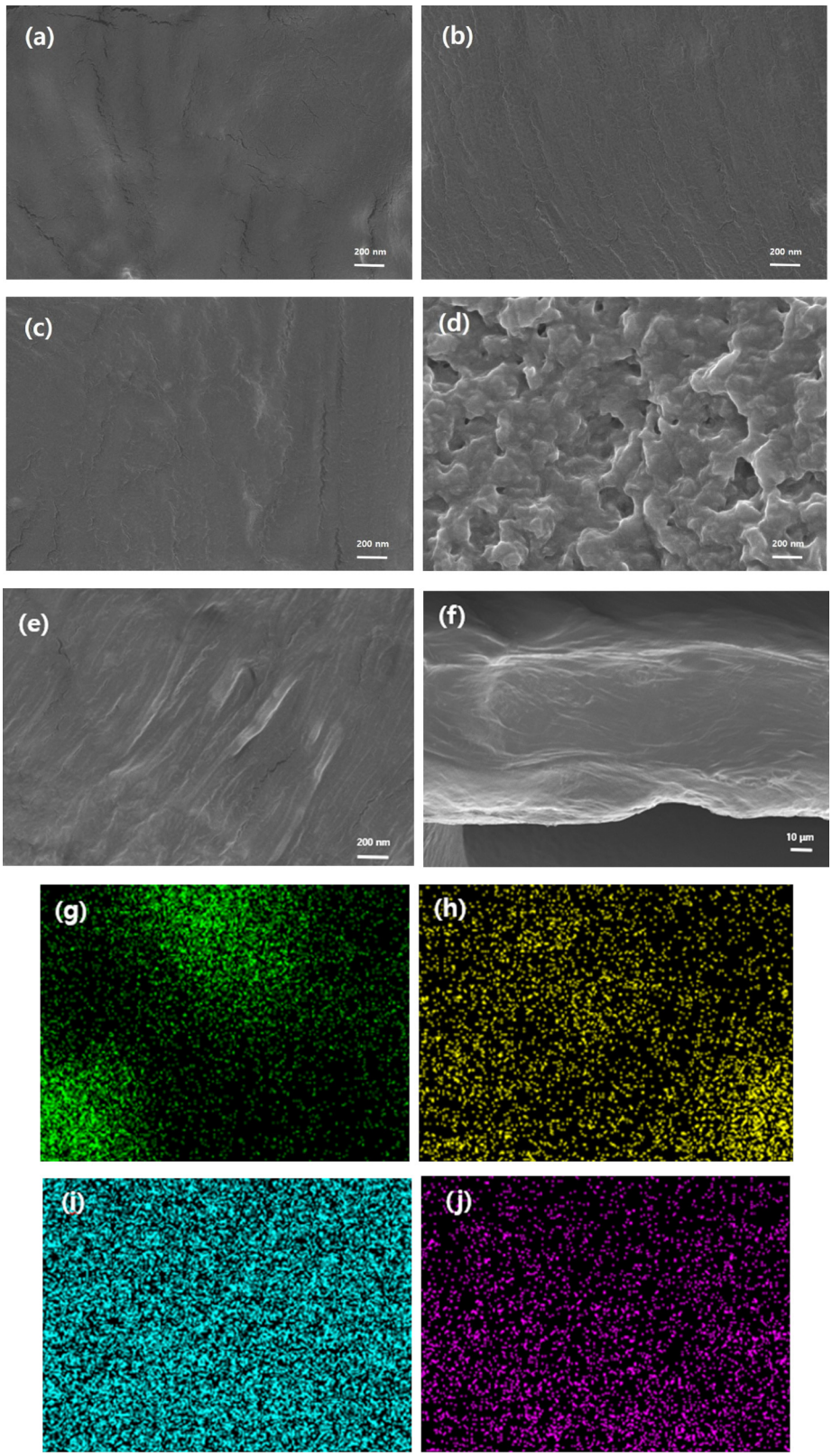

Fig. 2 SEM images of (a) CSE-01, (b) CSE-15, (c) CSE-110, (d) CSE-12, (e) CSE-p and (f) the cross-section of CSE-15. EDS elemental mapping images of (g) silicon in CSE-p and (h) silicon, (i) sulfur, and (j) fluorine in CSE-15.

resistance with the electrodes, and enhanced long-term cycling performance. Conversely, a high concentration of LiTFSI induced the formation of ion pairs or ionic aggregates, which hindered ionic conductivity and decreased electrochemical

stability. Therefore, the uniform dispersion of LiTFSI observed in the composite solid electrolytes contributed to good electrochemical performance.

Lithium-ion transport in solid polymer electrolytes occurs through the segmental motion of polymer chains. This segmental mobility is strongly influenced by the crystallinity of the polymer; thus, the efficiency of ion transport in solid-state batteries depends on the degree of crystallinity in the polymer matrix. To investigate how polymer blending ratios affect the crystallinity of the prepared composite solid electrolytes, XRD analysis was conducted. As shown in Fig. 3a, all CSE membranes exhibit similar XRD patterns, except for the CSE-01 sample. The PEO-based solid electrolytes displayed characteristic diffraction peaks at approximately 19° and 23°, which indicated the crystalline region of PEO. The sharpness and intensity of these peaks correlated with the degree of crystallinity. The CSE-01 sample, which contained no PAN, showed sharp and intense peaks, confirming a high degree of crystallinity. In contrast, as PAN was incorporated into the polymer matrix, a decrease in the intensity and sharpness of the crystalline peaks was observed, suggesting a reduction in crystallinity. This result indicated that PAN effectively disrupted the crystalline region of PEO when blended into the matrix. The trend became more pronounced with a high PAN content, and the CSE-12 sample containing the highest PAN content exhibited the weakest diffraction peaks, indicating the lowest crystallinity among the samples.

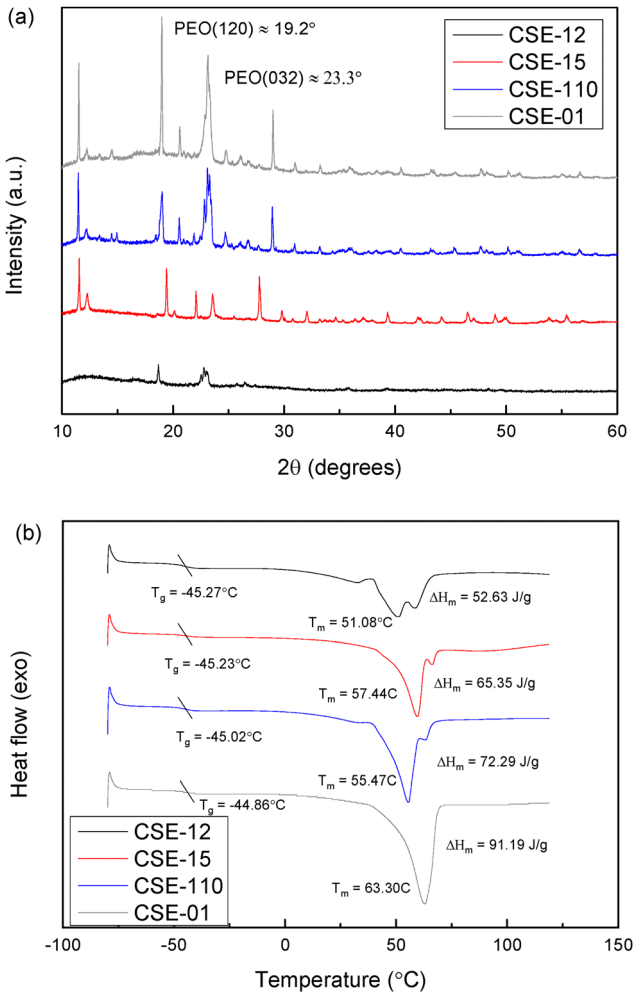

Fig. 3 (a) XRD patterns of the CSE membranes. (b) DSC curves of the CSE membranes.

The thermal behavior of the prepared CSEs was further investigated by DSC, which provided information on the glass transition temperature (T_g), melting temperature (T_m), and enthalpy of fusion (ΔH_m). These thermal properties are critical for evaluating the stability and performance of solid electrolytes in battery applications. The glass transition temperature represents the threshold at which the polymer transitions from a rigid glassy state to a more flexible rubbery state. Polymer chain mobility is minimal below T_g, whereas segmental motion is activated above T_g, facilitating the formation of conductive pathways for lithium-ion transport. A decrease in crystallinity and an increase in amorphous content decrease T_g. As presented in Fig. 3b, T_g exhibited only minor variations of less than 1 °C depending on the PAN content, with values of −44.86 °C, −45.02 °C, −45.23 °C, and −45.27 °C corresponding to CSE-01, CSE-110, CSE-15, and CSE-12, respectively. However, the differences between the samples were not significant. This was likely because PEO already possessed a relatively low T_g, making it less sensitive to the addition of PAN. This suggested that, although T_g was closely related to the segmental mobility of polymer chains in the amorphous region, the temperature at which this motion began did not differ significantly among the samples. However, an increased amorphous region implied that more polymer chains were available to participate in segmental motion. T_m, corresponding to the temperature at which crystalline regions melt and the intermolecular interactions between polymer chains break down, also showed little variation among the samples. The melting temperatures of CSE-01, CSE-110, CSE-15, and CSE-12 were determined from the DSC curves to be 51.08 °C, 57.44 °C, 55.47 °C, and 63.03 °C, respectively. The peaks for samples containing PAN in the T_m region split into two distinct peaks. The separation became more evident as the amount of PAN added increased. ΔH_m, the energy required to melt the crystalline regions, varied significantly, with values of 91.19, 72.29, 65.35, and 52.63 J g^{-1} for CSE-01, CSE-110, CSE-15, and CSE-12, respectively. Since ΔH_m reflects the degree of crystallinity, a high value corresponds to a great proportion of crystalline regions. As shown in Fig. 3b, CSE-01 displays the highest ΔH_m, indicating the highest crystallinity, whereas CSE-12 exhibits the lowest ΔH_m, consistent with the XRD results. These thermal transition trends and calculated enthalpy values were consistently observed across multiple independent measurements. These observations indicated that increasing the PAN content disrupted the regular arrangement of the PEO chains, thereby suppressing crystallization and increasing the amorphous regions within the polymer matrix.

An increased proportion of amorphous phases allows for more polymer chain movement, which induces faster Li^+ hopping and thereby enhances ionic conductivity. In other words, polymer chain flexibility increases as crystallinity decreases, providing Li^+ ions with greater freedom to migrate along ether

oxygen coordination sites. As a result, ionic conductivity within the solid electrolyte is directly improved. This relationship is a commonly observed trend in the ionic conductivity behavior of solid electrolytes, suggesting that controlling crystallinity is a key factor in electrolyte design. Based on the XRD and DSC results, CSE-12 had the highest amorphous regions and thus provided a favorable environment for lithium-ion transport due to the increased segmental motion of polymer chains. However, SEM analysis revealed that CSE-12 exhibited a rough and porous surface morphology, resulting from phase separation and microstructural instability due to the excessive PAN content. Such structural irregularities can interrupt continuous ion-transport pathways and reduce the mechanical strength and electrochemical stability of the electrolyte. While the addition of PAN effectively suppresses crystallinity and positively influences ionic conductivity, an excessive amount adversely affects the overall performance of the electrolyte. In conclusion, CSE-12 was advantageous in terms of crystallinity suppression but exhibited drawbacks in microstructural stability. Considering these factors, CSE-15 and CSE-110 were expected to offer a more optimal balance between crystallinity and structural stability, resulting in superior electrolyte performance.

In addition to the crystallinity of the polymer, the dissociation of the LiTFSI lithium salt within the electrolyte is a critical factor in achieving high ionic conductivity. This dissociation strongly depends on the interactions among the components of the composite solid electrolyte, namely PEO, PAN, SiO_2, and LiTFSI. Functional groups, such as the ether oxygen (C–O–C) in PEO, the nitrile group (C$\equiv$N) in PAN, and the surface hydroxyl groups (O–H) in SiO_2, interact with Li^+ ions, facilitating ion pair dissociation and the formation of efficient Li^+ conduction paths.

FT-IR spectroscopy was used to investigate the molecular structure and composition of the materials, as well as to evaluate the intermolecular interactions within the composite solid electrolyte. It also provided indirect evidence of lithium salt dissociation. This trend was highly reproducible and consistently observed in multiple independent samples. As shown in Fig. 4, the PEO matrix displays strong absorption peaks around 1100–1050 cm^{-1}, corresponding to the C–O–C ether bond, which plays a crucial role as a conduction site for Li^+ transport along the polymer backbone. In samples containing PAN, a characteristic stretching vibration of the nitrile group (C$\equiv$N) appeared near 2240 cm^{-1}, confirming the incorporation of the PAN polymer into the electrolyte (Fig. 4b). A distinct Si–O–Si stretching vibration peak for *in situ* SiO_2 formed *via* a sol–gel process was observed in the ranges of 1050–1070 cm^{-1} and 500–600 cm^{-1}, indicating the presence of inorganic nanofillers and their dispersion within the polymer matrix. The formation of SiO_2 was also confirmed by the peak around 3480 cm^{-1}, corresponding to the hydroxyl groups (O–H) on its surface, which interacted with Li^+ ions to afford conduction pathways (Fig. 4c). The obvious appearance of this peak suggested a strong interaction between the polymer and the inorganic component, as well as structural integration within the composite. When LiTFSI was incorporated into the polymer matrix, several characteristic peaks appeared in the FT-IR spectra. The symmetric and asymmetric stretching vibrations of S$=$O were observed near 1340 and 1140 cm^{-1}, respectively, while the vibrations of CF_3 groups were evident at approximately 1190 cm^{-1}. The variations in the position and intensity of these peaks with respect to the different PEO/PAN blending ratios reflected differences in the extent of lithium salt dissociation and ion pair formation.

These spectral shifts served as the indicators of the interaction strength between LiTFSI and the surrounding polymer or inorganic environment, which influenced the ionic conductivity of the solid electrolyte. The wavenumber range of 740–790 cm^{-1} in the FT-IR spectrum particularly indicated the dissociation of LiTFSI. The characteristic peak of ion-paired LiTFSI appeared near 760 cm^{-1} due to S$=$O and S–N stretching vibrations, whereas the free anionic form of $TFSI^-$ exhibited distinct peaks at 740 and 780 cm^{-1}. According to Fig. 4d, the distinct peak of the free anion, compared to the ion-pair peak in the CSE samples, indicates a high degree of lithium salt dissociation. This high salt dissociation stemmed from the effective dispersion of SiO_2 within the polymer matrix, achieved through the *in situ* hydrolysis process. The surface functional groups of the uniform-size and widespread SiO_2 particles strongly interacted with LiTFSI, promoting salt dissociation. The silanol (Si–OH) groups and oxygen atoms on the SiO_2 surface provided abundant electron pairs and acted as Lewis bases, strengthening Lewis acid–base interactions with Li^+ ions. This interaction promoted the dissociation of LiTFSI and a more uniform distribution of free lithium ions within the polymer matrix, thereby enhancing the availability of active hopping sites for Li^+ transport and contributing to improved ionic conductivity. The blending of PAN and PEO increased the amorphous content in the polymer matrix by suppressing PEO crystallinity. This led to enhanced chain mobility, which allowed the easy complexation of Li^+ ions with the ether oxygen (C–O–C) groups in the PEO chains. These effects facilitated the separation of LiTFSI into free ions and increased the number of effective ionic conduction paths in the composite electrolyte. The FT-IR results thus confirmed that strong interactions between the functional groups of PEO, PAN, SiO_2, and LiTFSI induced the dissociation of LiTFSI and increased the mobility of free Li^+ ions. This was closely related to the ionic conductivity of the electrolyte, as lithium salt dissociation increased the concentration of mobile lithium ions. In conclusion, the prepared CSE demonstrated a potential for high ionic conductivity due to a combination of factors: increased amorphous regions in the polymer matrix, enhanced polymer chain mobility, and effective interactions between lithium ions and fillers. The proposed mechanism is illustrated schematically in Fig. 5. The figure visualizes, at a molecular level, how the additives promote the amorphous structure of the polymer and LiTFSI dissociation *via* Lewis acid–base interactions, contributing to improved ionic transport within the composite solid electrolyte.

Ionic conductivity is a key parameter in evaluating the performance of electrolytes. To investigate the effect of polymer blending and in situ-incorporated SiO_2 on ionic conductivity,

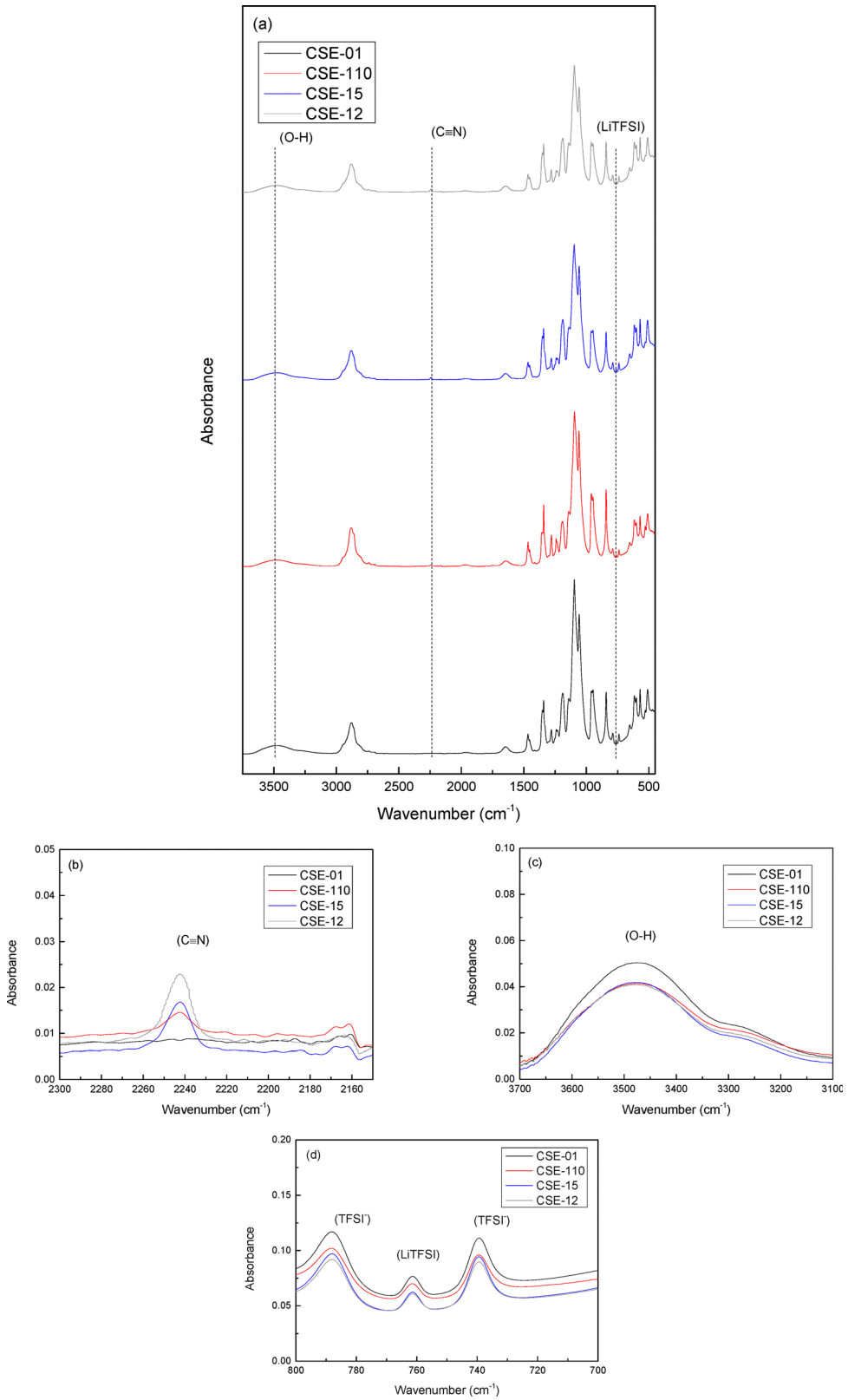

Fig. 4 FT-IR spectra of (a) the CSE membranes with their (b)–(d) enlarged view in specific wavenumber ranges.

symmetric stainless-steel cells (SS/CSE/SS) were assembled and analyzed using electrochemical impedance spectroscopy (EIS). Measurements were conducted at two different operating temperatures, 25 °C and 60 °C, to assess the impact of additive incorporation on the formation of electrolytes with fast ion transport characteristics. The resulting Nyquist plots displayed

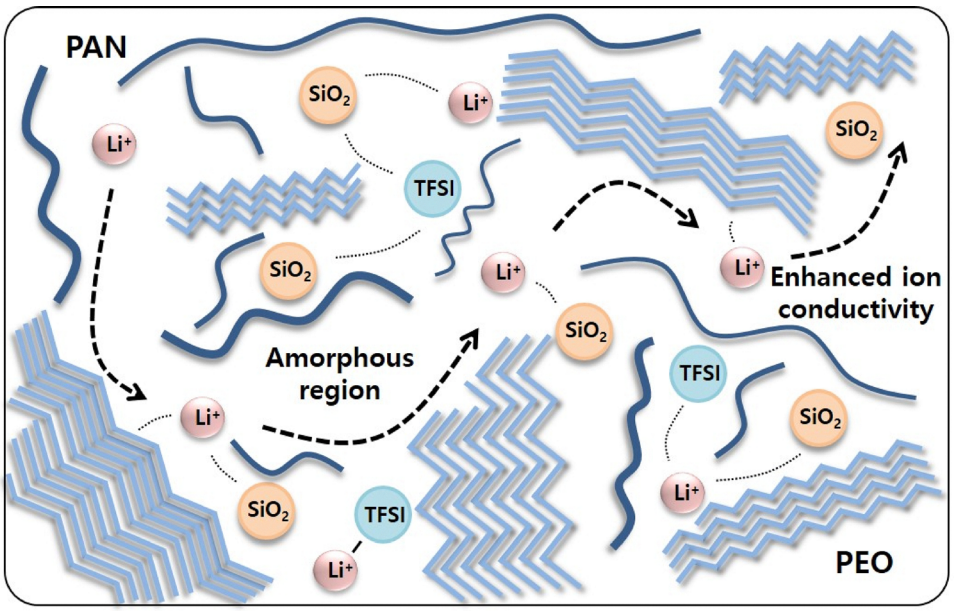

Fig. 5 Schematic of the ion-transfer mechanism in the CSE membrane.

the real impedance (Z') on the x-axis and the imaginary impedance (Z'') on the y-axis (Fig. 6). The intersection point of the plot with the x-axis in the high-frequency region was considered to represent the electrolyte resistance (R_s), which was used to calculate the ionic conductivity (σ) using eqn (1). The ionic conductivities of CSE-01, CSE-110, CSE-15, and CSE-12 at room temperature were 2.52×10^{-5} S cm^{-1}, 6.12×10^{-5} S cm^{-1}, 8.39×10^{-5} S cm^{-1}, and 5.47×10^{-5} S cm^{-1}, respectively.

In general, the ionic conductivity increases with temperature due to enhanced polymer chain mobility and weakened interactions between lithium ions and the polymer matrix, causing Li^+ ion transport. All samples exhibited increased ionic conductivity at high temperatures. The ionic conductivities of CSE-01, CSE-110, CSE-15, and CSE-12 at 60 °C increased to 7.54×10^{-5} S cm^{-1}, 2.56×10^{-4} S cm^{-1}, 3.81×10^{-4} S cm^{-1}, and 1.96×10^{-4} S cm^{-1}, respectively. Among the samples, CSE-01,

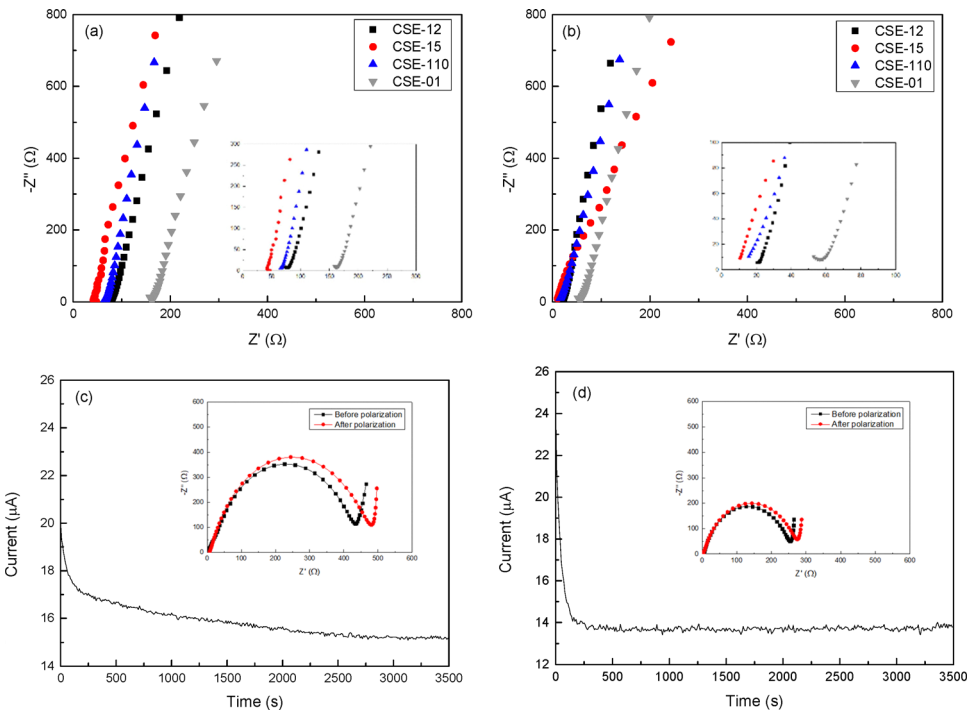

Fig. 6 Nyquist plots of the CSE membranes at (a) 25 °C and (b) 60 °C. Insets: Magnified regions at high frequencies. Chronoamperometry curves of (c) CSE-01 and (d) CSE-15. Insets: AC impedance spectra before and after polarization.

prepared without PAN, consistently exhibited the lowest ionic conductivity at both temperatures. Conversely, samples containing PAN showed enhanced ionic conductivity because of improved polymer segmental mobility, which arose from a suppressed polymer crystallinity and increased amorphous phase. A high degree of amorphous content afforded high chain flexibility, enabling Li^+ ions to hop more efficiently between active sites and thereby significantly improving ionic conductivity. In the case of CSE-12, containing the highest PAN content, although the conductivity was improved compared to CSE-01, the enhancement was limited. This limitation was due to structural defects, such as phase separation, heterogeneous microstructure, and micropores, caused by excessive PAN addition. As a result, the relative order of ionic conductivity among the samples was as follows: CSE-01 < CSE-12 < CSE-110 < CSE-15. These results indicated that optimizing the blending ratio of PAN and PEO was crucial for enhancing electrolyte performance. Furthermore, the ionic conductivity of the electrolyte was not only influenced by the polymer matrix structure, but also by interactions with inorganic nanoparticles. In particular, SiO_2 introduced *via* an *in situ* approach provided additional benefits. The incorporation of uniformly dispersed nanoscale SiO_2 particles suppressed the crystallinity of the polymer electrolyte and enhanced its mechanical strength, as well as promoting the formation of effective ion transport pathways at multiple interfaces between the polymer and inorganic components. This structural modification led to an increase in ionic active sites and a more continuous ion-conduction network. In conclusion, the incorporation and uniform dispersion of SiO_2 *via* the *in situ* method contributed to an enhanced mechanical stability and a more homogeneous electrolyte structure, which were beneficial for maintaining electrochemical performance.

The lithium-ion transference number (t_{Li^+}) plays a crucial role in evaluating both the ionic conductivity and ion selectivity of an electrolyte. A high lithium-ion transference number indicates superior electrolyte performance and is important for enhancing the efficiency of lithium-ion batteries. Symmetric Li/CSE/Li cells were assembled to investigate the intrinsic Li^+ mobility, and a constant polarization voltage was applied until a steady-state current was reached. Fig. 6c and d presents the current *versus* time polarization profiles, with the inset displaying the AC impedance spectra obtained before and after polarization. The chronoamperometry curve presented in Fig. 6d exhibits minor current oscillations during the polarization process. These slight signal irregularities were interpreted as a temporary effect during the initial polarization phase, rather than a sign of electrochemical instability. This behavior was likely due to minor interfacial adjustments at the electrode–electrolyte interface during Li^+ transport, such as transient polarization, interfacial resistance changes, or micro-scale inhomogeneities in the electrolyte. Significantly, these oscillations did not indicate the onset of lithium dendrite nucleation as the signal progressively stabilized upon reaching the steady-state current. This suggested that the observed behavior represented a transient adjustment of the rigid solid-state interface, a conclusion further supported by the stable long-term cycling performance, where no evidence of short circuit was observed. In the case of CSE-15, the addition of PAN slightly reduced the electrolyte viscosity while introducing a minor increase in mechanical rigidity, which may slightly induce local inhomogeneities at the electrode–electrolyte interface and result in the observed fluctuations. The t_{Li^+} values were calculated using eqn (2), resulting in values of 0.36 for CSE-15 and 0.24 for CSE-01. This result suggested that lithium ions migrated more efficiently in the CSE-15 sample compared to CSE-01, causing a higher lithium-ion transference number. It provided insight into the sequential enhancement mechanism: *in situ* SiO_2 nanoparticles first improved Li^+ transport by creating stable ion-conduction pathways within the PEO matrix, partially increasing the transference number, and the subsequent incorporation of PAN further promoted Li^+ mobility by reducing polymer crystallinity and enhancing segmental motion. As a result, lithium-ion transport became more efficient. This finding was consistent with the previously discussed ionic conductivity results, wherein increased conductivity alleviated the polarization at the electrode–electrolyte interface and facilitated more effective lithium-ion migration. Additionally, the uniformly dispersed nanoscale SiO_2 structures within the polymer matrix reinforced the structural durability of the electrolyte and assisted in developing interconnected ion pathways. Overall, this stepwise combination of SiO_2 and PAN allowed for progressively optimized lithium-ion movement throughout the electrolyte.

It is required to maintain good interfacial contact with the electrodes and ensure interfacial stability for the effective performance of electrolytes in lithium batteries. The interfacial stability prevents electrode corrosion and decomposition, thereby avoiding degradation in battery performance. Moreover, a wide and stable electrochemical window is essential for operation under high voltage conditions, as it is helpful in ensuring battery safety and long-term cycling performance. The oxidative stability of the electrolyte was investigated by LSV in asymmetric SS/electrolyte/Li cells. In the LSV test, the voltage was linearly increased while the corresponding current was recorded, and the point at which the current sharply increased indicated the oxidative decomposition voltage of the electrolyte. At this point, the electrolyte began to oxidize, followed by chemical degradation and performance deterioration. As shown in Fig. 7a, the oxidative decomposition voltages of the cells based on PEO and CSE-01 are approximately 3.4 V and 4.0 V (*vs.* Li/Li^+), respectively. By comparison, the cell incorporating CSE-15 exhibited a higher decomposition voltage of 4.5 V (*vs.* Li/Li^+). This enhancement in oxidative stability was ascribed to the synergistic effects of *in situ*-generated SiO_2 and PAN within the composite solid electrolyte. The *in situ*-formed SiO_2 improved interfacial stability with the polymer matrix and reinforced mechanical strength by establishing strong interactions. In addition, the incorporation of PAN reduced the crystallinity of the polymer, increasing chain mobility and ionic conductivity. These combined effects delayed the onset of oxidative reactions, maintaining electrochemical stability under high-voltage conditions. Consequently, the composite solid electrolyte manifested superior oxidative resistance and was well-suited for application under high voltage conditions.

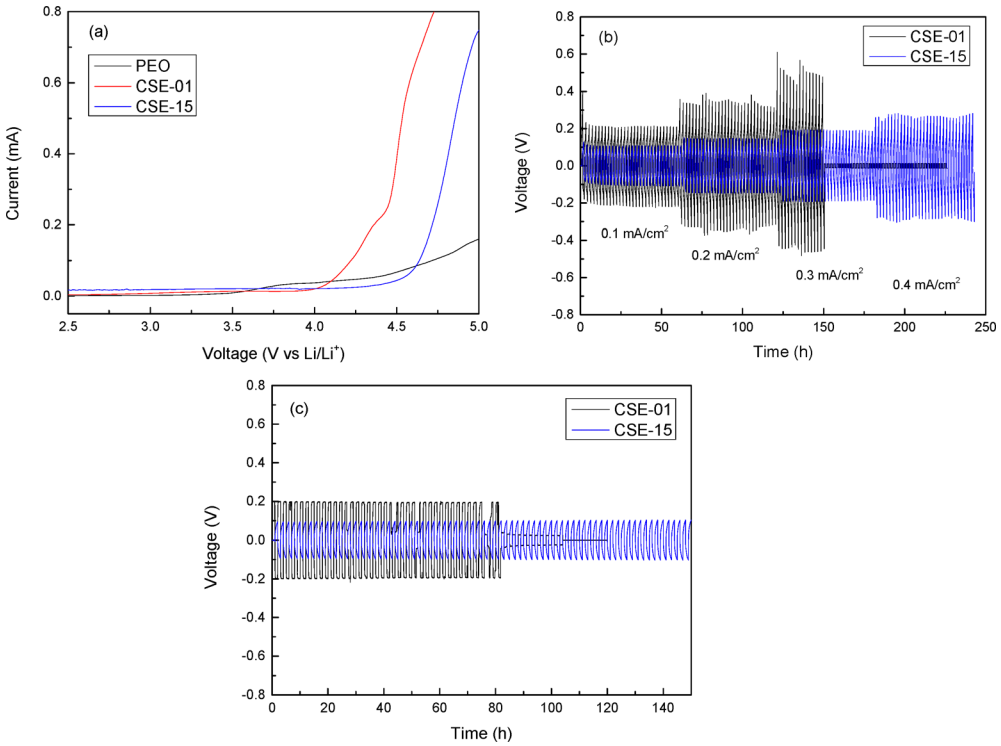

Fig. 7 (a) LSV curves of different membranes. (b) Critical current density measurements of the Li symmetric cells. (c) Li plating/stripping reversibility of the Li symmetric cells at a current density of 0.1 mA cm^{-2}.

The cycling performance and the interfacial stability between the electrolyte and lithium metal are critical indicators of long-term cycle life and reliable operation in all-solid-state batteries. Symmetric Li/CSE/Li cells were assembled and tested under galvanostatic charge–discharge conditions at various current densities to investigate the lithium plating and stripping behavior. As presented in Fig. 7b, a remarkable difference in critical current density was observed depending on the presence of PAN. The Li/CSE-01/Li cell exhibited significant polarization from the initial cycles, which was related to irregular voltage fluctuations during the lithium plating and stripping processes. On the other hand, the CSE-15 cell containing PAN and *in situ* SiO_2 provided a stable cycling behavior up to a current density of 0.4 mA cm^{-2}. The cell using CSE-01 without PAN experienced a sharp voltage drop and short-circuit failure at a current density of 0.3 mA cm^{-2}. This sudden voltage drop resulted from an internal short circuit caused by the formation of lithium dendrites and penetration through the solid electrolyte in the cell. Poor interfacial contact between the lithium metal and the electrolyte induced uneven lithium deposition and irregular dendritic growth, ultimately leading to chemical instability. However, the presence of PAN in the electrolyte contributed to enhanced ionic conductivity, and the incorporation of SiO_2 improved mechanical strength and chemical stability. These effects improved interfacial stability and resulted in stable lithium plating and stripping behavior. The stable interfacial behavior observed in the CSE-15 electrolyte indicated the effective inhibition of lithium dendrite formation and confirmed the superior mechanical and electrochemical properties. As illustrated in Fig. 7c, the CSE-15-based cell maintained stable operation for over 100 h at a current density of 0.1 mA cm^{-2} without significant polarization or short circuit. The consistency of this prolonged cycling was confirmed, with all CSE-15 samples consistently outperforming the others. In contrast, the cell using CSE-01 showed large polarization after 80 h, followed by a voltage drop. These results clearly demonstrated that the addition of PAN and *in situ* SiO_2 was positively helpful in lithium-ion transport and lithium deposition behavior. Therefore, it suppressed dendrite formation and promoted long-term interfacial stability in solid-state lithium batteries.

In order to evaluate the electrochemical performance of the composite solid electrolyte in a practical battery configuration, full cells were assembled, with $LiFePO_4$ (LFP) as the cathode and lithium metal as the anode, and tested at 60 °C. The cycling and rate performance were evaluated at 60 °C to ensure sufficient ionic conductivity, providing clear insights into the intrinsic behavior of CSE-15 and its response to PAN and *in situ* SiO_2 incorporation. To ensure the reliability of the long-term evaluation, multiple cells were fabricated for each composition, and preliminary tests confirmed highly consistent electrochemical trends across different batches. The following results represent the performance of optimized, representative cells. According to Fig. 8a, the cell with the CSE-15 electrolyte exhibits prolonged and highly stable cycling performance over 150 cycles at a current rate of 0.5C. During the charge–discharge process, the cell delivered a high specific discharge capacity of 151.4 mA h g^{-1} and an excellent Coulombic efficiency of 99.8%. These findings confirmed the outstanding electrochemical

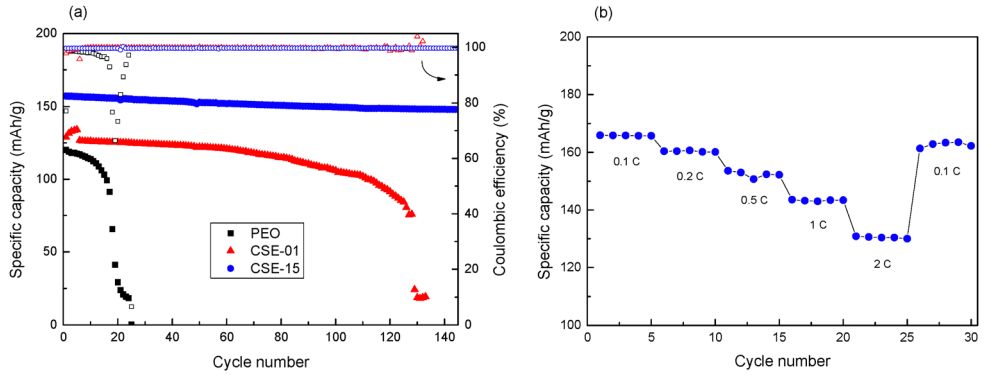

Fig. 8 (a) Cycling performance and Coulombic efficiency of the membranes at 0.5C and 60 °C. (b) Rate performance of CSE-15 at various values of current.

reversibility and long-term cycling stability of the cell. On the other hand, the cell using CSE-01 without PAN displayed an initial discharge capacity of approximately 130 mA h g^{-1}, but this capacity began to significantly decline after about 60 cycles, and instability in Coulombic efficiency was also observed. The cell using pure PEO also showed rapid capacity fading from the early cycles and unstable Coulombic efficiency, dropping below 80%. Despite the identical electrode configurations, performance differences were observed due to the properties of the electrolytes. The poor mechanical strength and chemical instability of the PEO and CSE-01 electrolytes failed to effectively suppress lithium dendrite formation and caused unstable interfacial contact with the electrodes. However, the CSE-15 electrolyte provided remarkably improved cycling stability, which was ascribed to the synergistic effects of *in situ* dispersed SiO_2 nanoparticles and PAN incorporation. The presence of these components gave rise to the enhancement of the mechanical integrity and high ionic conductivity of the electrolyte, increasing the stability of the cell. The rate capability of the cells was also evaluated at various current rates. The battery based on CSE-15 delivered discharge capacities of 165.9, 160.4, 152.3, 143.3, and 130.4 mA h g^{-1} at 0.1C, 0.2C, 0.5C, 1C, and 2C, respectively, as presented in Fig. 8b. When the current rate was returned to 0.1C, the cell recovered approximately 98% of its initial discharge capacity. It confirmed the excellent cycling stability and high reversibility of the cell. These results demonstrated that the CSE-15 electrolyte maintained electrochemical stability without significant degradation across a wide range of current densities. This was attributed to the excellent mechanical strength and chemical stability of the CSE-15 electrolyte, which helped to maintain interfacial stability with the electrodes and supported efficient lithium-ion conduction and uniform lithium plating.

4. Conclusion

In this study, a high-performance composite solid polymer electrolyte was developed by blending PEO with PAN and incorporating SiO_2 nanoparticles *via* the *in situ* sol–gel method. This combination synergistically enhanced both electrochemical and mechanical properties, overcoming the critical limitations of conventional polymer electrolytes in all-solid-state lithium batteries. Optimized PAN content suppressed PEO crystallinity, thereby increasing amorphous regions and segmental chain mobility without causing phase separation or microstructural defects. The optimized composition (CSE-15) successfully achieved a balance between ionic conductivity and structural integrity. The *in situ* SiO_2 formed through the hydrolysis of TEOS was uniformly dispersed, expanding the amorphous regions, reinforcing the polymer network, and facilitating interconnected ion-transport pathways. Furthermore, the strong Lewis base sites on SiO_2 promoted lithium-salt dissociation, resulting in a high lithium-ion transference number of 0.36. Electrochemical characterization confirmed that the optimized composite electrolyte (CSE-15) delivered an outstanding performance. It exhibited a high ionic conductivity of 3.81×10^{-4} S cm^{-1} at 60 °C, along with excellent interfacial compatibility and mechanical durability. The cell displayed stable lithium plating/stripping behavior for over 100 h without dendrite formation or short-circuit failure. In full cell configurations with $LiFePO_4$ and lithium metal, the cell maintained a high discharge capacity of 151.4 mA h g^{-1} and a Coulombic efficiency of 99.8% over 150 cycles at 0.5C. The electrolyte also showed excellent rate capability and capacity recovery, indicating its robustness across varying current densities.

In summary, a composite solid electrolyte membrane composed of in situ-generated SiO_2, PEO, and PAN was successfully prepared and comprehensively analyzed. The dual incorporation of PAN and SiO_2 into the PEO matrix proved highly effective in enhancing ionic conductivity, mechanical properties, and electrochemical stability. This work demonstrated that the rational design of composite electrolytes using polymer blending and *in situ* filler integration offered a promising strategy for overcoming the limitations of conventional polymer electrolytes. Moreover, the wide electrochemical stability window of CSE-15 suggested a strong potential for future integration with high-voltage cathode materials, expanding its applicability beyond the scope of this study. Therefore, the developed CSE represents a viable and scalable solution for all-solid-state lithium batteries requiring high performance, safety, and long-term cycling stability.

Author contributions

Hun Lee: writing – original draft, methodology, formal analysis, data curation, visualization, investigation, and conceptualization. Sung Yeon Hwang: writing – review and editing, validation, supervision, resources, and conceptualization.

Conflicts of interest

The authors declare that they have no known competing financial interests or personal relationships that could have appeared to influence the work reported in this paper.

Data availability

Data will be made available upon request.

Acknowledgements

This work was supported by the Technology Development Program (RS-2025-25435993, 20008628, RS-2024-00507722 and RS-2024-00432206) funded by the Ministry of Trade, Industry and Energy (MOTIE, Republic of Korea).

References

1 G. Berckmans, M. Messagie, J. Smekens, N. Omar, L. Vanhaverbeke and J. V. Mierlo, Cost Projection of State of the Art Lithium-Ion Batteries for Electric Vehicles Up to 2030, *Energies*, 2017, **10**, 1314.
2 S. Luiso and P. Fedikiw, Lithium-ion battery separators: Recent developments and state of art, *Curr. Opin. Electrochem.*, 2020, **20**, 99–107.
3 Y. Zhao, L. Geng, W. Meng and J. Ye, Low-Temperature Electrolytes for Lithium-Ion Batteries: Current Challenges, Development, and Perspectives, *Nano-Micro Lett.*, 2026, **18**, 65.
4 D. Miranda, R. Goncalves, S. Wuttke, C. M. Costa and S. Lanceros-Mendez, Overview on Theoretical Simulations of Lithium-Ion Batteries and Their Application to Battery Separators, *Adv. Energy Mater.*, 2023, **13**, 2203874.
5 H. Lee, M. Yanilmaz, O. Toprakci, K. Fu and X. Zhang, A review of recent developments in membrane separators for rechargeable lithium-ion batteries, *Energy Environ. Sci.*, 2014, **7**, 3857.
6 A. Li, A. C. Y. Yuen, W. Wang, I. M. D. C. Cordeiro, C. Wang, T. B. Y. Chen, J. Zhang, Q. N. Chan and G. H. Yeoh, A Review on Lithium-Ion Battery Separators towards Enhanced Safety Performances and Modelling Approaches, *Molecules*, 2021, **26**, 478.
7 C. J. Weber, S. Geiger, S. Falusi and M. Roth, Material Review of Li Ion Battery Separators, *AIP Conf. Proc.*, 2014, **1597**, 66–81.
8 C. F. J. Francis, I. L. Kyratzis and A. S. Best, Lithium-Ion Battery Separators for Ionic-Liquid Electrolytes: A Review, *Adv. Mater.*, 2020, **32**, 1904205.
9 I. T. Adebanjo, J. Eko, A. G. Agbeyegbe, S. F. Yuk, S. V. Cowart, E. A. Nagelli, F. J. Burpo, J. L. Allen, D. T. Tran, N. Bhattarai, K. Shah, J. Y. Hwang and H. H. Sun, A comprehensive review of lithium-ion battery components degradation and operational considerations: a safety perspective, *Energy Adv.*, 2025, **4**, 820–877.
10 W. Zhao, J. Yl, P. He and H. Zhou, Solid-State Electrolytes for Lithium-Ion Batteries: Fundamentals, Challenges and Perspectives, *Electrochem. Energy Rev.*, 2019, **2**, 574–605.
11 Y. Zheng, Y. Yao, J. Ou, M. Li, D. Luo, H. Dou, Z. Li, K. Amine, A. Yu and Z. Chen, A review of composite solid state electrolytes for lithium batteries: Fundamentals, key materials and advanced structures, *Chem. Soc. Rev.*, 2020, **49**, 8790–8839.
12 X. Lu, Y. Wang, X. Xu, B. Yan, T. Wu and L. Lu, Polymer-Based Solid-State Electrolytes for High-Energy-Density Lithium-Ion Batteries-Review, *Adv. Energy Mater.*, 2023, **13**, 2301746.
13 L. Wang, J. Li, G. Lu, W. Li, Q. Tao, C. Shi, H. Jin, G. Chen and S. Wang, Fundamentals of electrolytes for solid-state batteries: challenges and perspectives, *Front. Mater.*, 2020, **7**, 111.
14 Z. Karkar, M. S. E. Houache, C. H. Yim and Y. Abu-Lebdeh, An industrial perspective and intellectual property landscape on solid-state battery technology with a focus on solid-state electrolyte chemistries, *Batteries*, 2024, **10**, 24.
15 S. Wang, A. L. Monaca and G. P. Demopoulos, Composite solid-state electrolytes for all solidstate lithium batteries: progress, challenges and outlook, *Energy Adv.*, 2025, **4**, 11–36.
16 M. Kathiresan, A. K. Lakshmi, N. Angulakshmi, S. Garcia-Ballesteros, F. Bella and A. M. Stephan, Viologen as an Electrolyte Additive for Extreme Fast Charging of Lithium-Ion Batteries, *Battery Energy*, 2025, **4**, e20240039.
17 L. A. Kumar, M. Kathiresan, S. Alwarappan, F. Bella and A. M. Stephan, Fast Charging of Lithium-Ion Batteries by the Effective Formulation of Nonaqueous Liquid Electrolytes, *J. Phys. Chem. C*, 2025, **129**, 9980–9991.
18 C. Li, R. Li, K. Liu, R. Si, Z. Zhang and Y. S. Hu, NaSICON: a promising solid electrolyte for solid-state sodium batteries, *Interdisciplinary Mater.*, 2022, **1**, 396–416.
19 Z. Jiang, S. Wang, X. Chen, W. Yang, X. Yao, X. Hu, Q. Han and H. Wang, Tape-Casting Li0.34La0.56TiO3 Ceramic Electrolyte Films Permit High Energy Density of Lithium-Metal Batteries, *Adv. Mater.*, 2020, **32**, 1906221.
20 D. Campanella, D. Belanger and A. Paolella, Beyond garnets, phosphates and phosphosulfides solid electrolytes: New ceramic perspectives for all solid lithium metal batteries, *J. Power Sources*, 2021, **482**, 228949.
21 L. Xu, J. Li, W. Deng, H. Shuai, S. Li, Z. Xu, J. Li, H. Hou, H. Peng, G. Zou and X. Ji, Garnet solid electrolyte for advanced all-solid-state Li batteries, *Adv. Energy Mater.*, 2021, **11**, 2000648.
22 F. Oksuzoglu, S. Ates, O. M. Ozkendir, G. Celik, Y. R. Eker and H. Baveghar, Structure and ionic conductivity of NASICON-type LATP solid electrolyte synthesized by the solid-state method, *Ceram. Int.*, 2024, **50**, 31435–31441.

23 J. Lu and Y. Li, Perovskite-type Li-ion solid electrolytes: a review, *J. Mater. Sci.: Mater. Electron.*, 2021, **32**, 9736–9754.
24 B. Tao, C. Ren, H. Li, B. Liu, X. Jia, X. Dong, S. Zhang and H. Chang, Thio-/LISICON and LGPS-type solid electrolytes for all-solid-state lithium-ion batteries, *Adv. Funct. Mater.*, 2022, **32**, 2203551.
25 G. Xi, M. Xiao, S. Wang, D. Han, Y. Li and Y. Meng, Polymer-based solid electrolytes: material selection, design, and application, *Adv. Funct. Mater.*, 2021, **31**, 2007598.
26 D. M. Reinoso and M. A. Frechero, Strategies for rational design of polymer-based solid electrolytes for advanced lithium energy storage applications, *Energy Storage Mater.*, 2022, **52**, 430–464.
27 M. Chen, Z. Yue, Y. Wu, Y. Wang, Y. Li and Z. Chen, Thermal stable polymer-based solid electrolytes: Design strategies and corresponding stable mechanisms for solid-state Li metal batteries, *Sustainable Mater. Technol.*, 2023, **36**, e00587.
28 A. Murali, M. Sakar, S. Priya, V. Vijayavarman, S. Pandey, R. Sai, Y. Katayama, M. A. Kader and K. Ramanujam, Insights into the emerging alternative polymer-based electrolytes for all solid-state lithium-ion batteries: A review, *Mater. Lett.*, 2022, **313**, 131764.
29 F. A. Amaral, R. M. Sousa, L. C. T. Morais, R. G. Rocha, I. O. Campos, W. S. Fagundes, C. N. P. Fonseca and S. C. Canobre, Preparation and characterization of the porous solid polymer electrolyte of PAN/PVA by phase inversion, *J. Appl. Electrochem.*, 2015, **45**, 809–820.
30 Y. Ma, J. Wan, Y. Yang, Y. Ye, X. Xiao, D. T. Boyle, W. Burke, Z. Huang, H. Chen, Y. Cui, Z. Yu, S. T. Oyakhire and Y. Cui, Scalable, ultrathin, and high-temperature-resistant solid polymer electrolytes for energy-dense lithium metal batteries, *Adv. Energy Mater.*, 2022, **12**, 2103720.
31 P. Yadav, M. S. Hosen, P. K. Dammala, P. Ivanchenko, J. V. Mierlo and M. Berecibar, Development of composite solid polymer electrolyte for solid-state lithium battery: Incorporating LLZTO in PVDF-HFP/LiTFSI, *Solid State Ion.*, 2023, **399**, 116308.
32 L. Yang, Z. Wang, Y. Feng, R. Tan, Y. Zuo, R. Gao, Y. Zhao, L. Han, Z. Wang and F. Pan, Flexible Composite Solid Electrolyte Facilitating Highly Stable ''Soft Contacting'' Li–Electrolyte Interface for Solid State Lithium-Ion Batteries, *Adv. Energy Mater.*, 2017, **7**, 1701437.
33 P. Yao, H. Yu, Z. Ding, Y. Liu, J. Lu, M. Lavorgna, J. Wu and X. Liu, Review on polymer-based composite electrolytes for lithium batteries, *Front. Chem.*, 2019, **7**, 522.
34 X. Tan, Y. Wu, W. Tang, S. Song, J. Yao, Z. Wen, L. Lu, S. V. Savilov, N. Hu and J. Molenda, Preparation of Nanocomposite Polymer Electrolyte via In Situ Synthesis of SiO_2 Nanoparticles in PEO, *Nanomaterials*, 2020, **10**, 157.
35 D. Lin, W. Liu, Y. Liu, H. R. Lee, P. C. Hsu, K. Liu and Y. Cui, High Ionic Conductivity of Composite Solid Polymer Electrolyte via In Situ Synthesis of Monodispersed SiO_2 Nanospheres in Poly(ethylene oxide), *Nano Lett.*, 2016, **16**, 459–465.
36 Y. Li, L. Yang, R. Dong, T. Zhang, J. Yuan, Y. Liu, Y. Liu, Y. Sun, B. Zhong, Y. Chen, Z. Wu and X. Guo, A high strength asymmetric polymer–inorganic composite solid electrolyte for solid-state Li-ion batteries, *Electrochim. Acta*, 2022, **404**, 139701.
37 K. Vignarooban, M. Dissanayake, I. Albinsson and B. E. Mellander, Effect of TiO_2 nano-filler and EC plasticizer on electrical and thermal properties of poly(ethylene oxide) (PEO) based solid polymer electrolytes, *Solid State Ion.*, 2014, **266**, 25–28.
38 Z. Cheng, T. Liu, B. Zhao, F. Shen, H. Jin and X. Han, Recent advances in organic-inorganic composite solid electrolytes for all-solid-state lithium batteries, *Energy Storage Mater.*, 2021, **34**, 388–416.
39 L. Li and Y. Duan, Engineering Polymer-Based Porous Membrane for Sustainable Lithium-Ion Battery Separators, *Polymers*, 2023, **15**, 3690.
40 W. B. Nassir, T. H. Mengesha, J. K. Chang, R. Jose and C. C. Yang, Multilayer hybrid solid-state electrolyte membrane for the high rate and long-life cycle performance of lithium-metal batteries, *Colloids Surf. A*, 2024, **691**, 133839.
41 H. Lee and D. Lee, Composite Membrane Containing Titania Nanofibers for Battery Separators Used in Lithium-Ion Batteries, *Membranes*, 2023, **13**, 499.
42 K. M. Anilkumar, B. Jinisha, M. Manoj and S. Jayalekshmi, Poly(ethylene oxide) (PEO) – Poly(vinyl pyrrolidone) (PVP) blend polymer based solid electrolyte membranes for developing solid state magnesium ion cells, *Eur. Polym. J.*, 2017, **89**, 249–262.
43 W. Lyu, G. He and T. Liu, PEO-LITFSI-SiO_2-SN System Promotes the Application of Polymer Electrolytes in All-Solid-State Lithium-ion Batteries, *ChemistryOpen*, 2020, **9**, 713–718.
44 J. Yang, C. Yi, M. Li, Z. Wu, J. Xia, Y. Li and J. Liu, Recent Advances in LATP/Polymer Composite Electrolytes for Solid-State Lithium Batteries, *Energy Environ. Mater.*, 2025, **0**, e70090.
45 N. Yazie, D. Worku, N. Gabbiye, A. Alemayehu, Z. Getahun and M. Dagnew, Development of polymer blend electrolytes for battery systems: recent progress, challenges, and future outlook, *Mater. Renewable Sustainable Energy*, 2023, **12**, 73–94.
46 J. Feng, L. Wang, Y. Chen, P. Wang, H. Zhang and X. He, PEO based polymer-ceramic hybrid solid electrolytes: a review, *Nano Converg.*, 2021, **8**, 2.
47 C. R. M. Pila, E. P. Cappe, N. D. S. Mohallem, O. L. Alves, M. A. A. Frutisd, N. Sanchez-Ramireze, R. M. Torresie, H. L. Ramireza and Y. M. Laffitaa, Effect of the LLTO nanoparticles on the conducting properties of PEO-based solid electrolyte, *Solid State Sci.*, 2019, **88**, 41–47.
48 Y. Xu, J. Li and W. Li, A Strategy for Preparing Solid Polymer Electrolytes Containing In Situ Synthesized ZnO Nanoparticles with Excellent Electrochemical Performance, *Nanomaterials*, 2022, **12**, 2680.
49 F. Croce and B. Scrosati, Nanocomposite Lithium Ion Conducting Membranes, *Ann. N. Y. Acad. Sci.*, 2003, **984**, 194–207.

50 M. K. Wilson, C. Augustin, A. Abhilash, B. Jinisha, A. Antony, M. K. Jayaraj and S. Jayalekshmi, Solid electrolyte membranes with Al_2O_3 nanofiller for fully solid-state Li-ion cells, *Polym. Bull.*, 2024, **81**, 6003–6024.
51 J. Fan and P. S. Fedkiw, Composite Electrolytes Prepared from Fumed Silica, Polyethylene Oxide Oligomers, and Lithium Salts, *J. Electrochem. Soc.*, 1997, **144**, 399–408.
52 B. Bera, D. S. Aaron and M. M. Mench, Factors controlling the performance of lithiummetal solid-state batteries with polyethylene oxide-based composite polymer electrolytes, *Energy Adv.*, 2026, **5**, 119–129.
53 Z. He, E. Dong, C. Li, J. Liu, Y. Jing, M. Yin, L. Wang, Y. Zhang, S. Liu, D. Wang, P. Yan, H. Liu, S. Dou and B. Wang, Phase-separated polymer electrolytes with dual-interface enhancement effect for high-loading lithium metal batteries, *J. Energy Chem.*, 2026, **116**, 504–513.
54 D. Pugliese, R. Staffieri and F. Bella, From materials to management: The expanding role of design of experiments in advanced battery technologies, *Energy Storage Mater.*, 2026, **85**, 104890.
55 N. Molinari, J. P. Mailoa and B. Kozinsky, Effect of Salt Concentration on Ion Clustering and Transport in Polymer Solid Electrolytes: A Molecular Dynamics Study of PEO–LiTFSI, *Chem. Mater.*, 2018, **30**, 6298–6306.
56 Q. Zhang, K. Liu, F. Ding and X. Liu, Recent advances in solid polymer electrolytes for lithium batteries, *Nano Res.*, 2017, **10**, 4139–4174.
57 J. Zhang, V. Perez, T. Garcia, D. Yoon, D. Wagner, Y. Schneider, M. H. Lee, S. J. Lee and D. Oh, Competing effects of low salt ratio on electrochemical performance and compressive modulus of PEO-LiTFSI/LLZTO composite electrolytes, *Energy Adv.*, 2024, **3**, 2820–2827.
58 B. K. Choi, Y. W. Kim and H. K. Shin, Ionic conduction in PEO–PAN blend polymer electrolytes, *Electrochim. Acta*, 2000, **45**, 1371–1374.
59 W. Chun-Guey, W. Chiung-Hui, L. Ming-I and C. Huey-Jan, New Solid Polymer Electrolytes Based on PEO/PAN Hybrids, *J. Appl. Polym. Sci.*, 2006, **99**, 1530–1540.
60 J. D. Kim, T. H. Hong and J. T. Lee, Compositional engineering of composite polymer electrolytes for all solid-state batteries to simultaneously improve reaction kinetics and long-term stability, *J. Power Sources*, 2024, **593**, 233982.
61 S. Z. Wang, J. Y. Lyu, W. He, P. J. Liu and Q. L. Yan, Thermal decomposition and combustion behavior of ion conductive PEO-PAN based energetic composites, *Combust. Flame*, 2021, **230**, 111421.